Ocean Systems Engineering, *Vol. 15, No. 4 (2025) 441-463*
https://doi.org/10.12989/ose.2025.15.4.441

Design sensitivities analysis for transient incompressible laminar flows using extended complex variable method

Mojtaba Sheikhi Azqandi[1] and Mahdi Hassanzadeh[*2]

[1]*Mechanical Engineering Department, University of Birjand, Birjand, Iran*
[2]*Department of Mechanical Engineering, Go.C., Islamic Azad University, Gorgan, Iran*

(Received September 23, 2024, Revised August 4, 2025, Accepted October 16, 2025)

Abstract. In the present study, the extended standard complex variable method (ESCVM) was proposed as a robust method for calculating the analysis of design sensitivities, including the first and second order. The standard complex variables method (SCVM) uses only the imaginary step for sensitivity analysis. In contrast, the presented method applies both the imaginary and the real part to enhance the effectiveness of the procedure. To illustrate this, the ESCVM is employed for the transited laminar incompressible flow. The Navier-Stokes equations are solved using finite element analysis and the developed SCVM was then applied to them. It has been shown that the first order (FO) sensitivity analysis is less susceptible to variations in the step size for both the standard and extended SCVM. However, it is evident that, unlike the SCVM, the extended SCVM was less dependent on the step size in estimating the second-order sensitivity (SO). This ability can be seen as an improvement in the efficiency and robustness of the extended standard method for complex variables.

Keywords: extended complex variables method; finite element analysis; incompressible laminar flows; Navier-Stokes equations; sensitivities analysis

1. Introduction

Sensitivity analysis is a unique and powerful means of disseminating engineering problems that uses the first derivative of an independent variable relative to the dependent variable to demonstrate how the dependent variable reacts to perturbations in one or more independent variables. This comparative measure of responsiveness provides an insight into the relationship between the two kinds of variables. A thorough overview of the different discrete techniques for computational derivatives is presented by Martins and Hwang (2013). in their thorough exposition, all of which is presented in a consistent mathematical framework.

Furthermore, this approach has numerous applications, encompassing the derivation of first- and second-order optimization techniques (Ta *et al.* 2018, Akkari *et al.* 2014), as well as providing an assessment of the uncertainty linked to the solution (Lamberi and Gosselin 2018). Additionally, sensitivity analysis proves to be an effective method for assessing how changes in design parameters influence flow responses, and it is utilized within the field of flow analysis.

∗Corresponding author, Assistant Professor, E-mail: mahdi_hassanzadeh@iau.ac.ir

http://www.techno-press.org/?journal=ose&subpage=7 ISSN: 2093-6702 (Print), 2093-677X (Online)

In classical optimization methods, it is necessary to calculate the sensitivity values of the objective function and constraints to the dependent variables. If precise methods for calculating sensitivity are applied in engineering problems that involve complex and extensive calculations (Sheikhi Azqandi *et al.* 2018, Sheikhi Azqandi 2021), gradient optimization methods can be used to achieve the optimal design, which requires calculating the derivative of the objective functions and problem constraints with respect to the design variables. Obtaining accurate values of the derivatives of the objective function with respect to the design variables (both first and second order) using SCVM and ESCVM methods serves as the basic input for gradient-based optimization algorithms. In these methods, such as steepest descent or other methods, the higher the accuracy of the sensitivity calculations, the faster the optimal point is found. In addition, if higher-order derivatives, such as the second-order derivative, are available, more powerful methods, such as Newton's method, can be used to reach the optimal point faster and with lower computational cost. The main point is that in problems that require simulation, the objective function itself and its derivatives are calculated numerically and approximately, and an inappropriate step size may change the accuracy of the results and their derivatives. However, if the ECVM method is used, the limitation of the small step size in calculating the sensitivity analysis is eliminated, and results can be obtained with a tiny step size, ensuring the accuracy of the results and their sensitivities. In this case, optimization methods can better and faster converge to the optimal solution.

Researchers can utilize various analytical methods to calculate sensitivity, including finite difference analysis, continuous sensitivity approach (Kavadias *et al.* 2015, Hu and Kozlowski 2018), complex differentiation method (Vincent and Bogey 2023), discrete sensitivity method (Liu *et al.* 2014, Ding *et al.* 2018), semi-analytic method (Sheikhi Azqandi and Hassanzadeh 2018), hyper dual numbers (Tanaka *et al.* 2015, Tanaka *et al.* 2016), complex variables method (Jafari and Jafari 2019, Voorhess *et al.* 2012, Sheikhi Azqandi *et al.* 2019), hybrid complex variables method and direct sensitivity method (Sheikhi Azqandi *et al.* 2020), and extended complex variables method (Sheikhi Azqandi and Hassanzadeh (2021)). The complex variables method (CVM) has gained popularity in recent studies due to its significant advantages. Squire and Trapp determined the derivatives of real functions using the complex variables method (Squire and Trapp 1998). Martins *et al.* (2003) applied the complex variables method approach to determine sensitivity for optimal design in three-dimensional aerospace structures. Furthermore, Martins *et al.* (2000), employed SCVM to estimate sensitivity in two-dimensional computational fluid dynamics. Ilinca *et al.* (2008) describe the formulations of the first-order (FO) and second-order (SO) sensitivity equation method and its applications to transient flow problems. Their research demonstrates solutions for both value and shape parameters using a three-dimensional solution algorithm.

In a study by Rodriguez (2000), the complex variable method was utilized in sensitivity analysis to determine the search direction in the optimization of aircraft inlet duct design. Similarly, Fiorini *et al.* (2021) conducted sensitivity analysis focusing on the Navier-Stokes equations.

When using the complex variable method to determine first-order sensitivity, it was found that the results are not affected by the step size. Therefore, if implemented correctly, this method can provide highly accurate design sensitivities (Burg and Newman 2003).

For most technical applications, FO derivatives are to be computed with the imaginary complex step. The SO derivatives estimations can be effectively done from the imaginary complex step alone. However, just like the finite-difference approach, making an attempt to narrow down the size of the step could bring round-off errors due to the inaccuracies associated with the process of subtraction.

Conversely, the larger the step size, the lower the precision of the calculations due to the truncation error. Consequently, there is a restricted range in which a reduction of the step size increases the accuracy. Consequently, a compromise between the rounding error and the truncation error should be considered when determining the SO sensitivity.

The traditional method for determining the FO derivatives can be extracted by the Taylor series with an imaginary complex step size (Lai and Crassidis 2008). The complex variables can be expressed by Euler's formula in trigonometric form. Therefore, the complex Taylor series can also be extended with angles. To determine the FO and SO derivatives, A set of Taylor series characterized by an angular difference of 180 degrees was used to derive more accurate equations for performing the sensitivity analysis (Lai and Crassidis 2008). As with the SCVM, the truncation error was reduced with this method and there was no rounding error in the new estimate of the FO derivative. In addition, the SO derivation provides a more accurate estimate of the round-off error. Based on the review of sources conducted by the authors, the proposed methods have not yet been applied to engineering problems. This research aims to overcome this weakness immediately.

This study introduces a novel application of the extended SCVM for the sensitivity analysis of transient laminar incompressible flow around a cylindrical barrier, with a focus on FO and SO effects.

First, the finite element method (FEM) was applied to analyze the flow regimes. Subsequently, the FO and SO sensitivities were calculated using the ESCVM. Then a comparison is made between the ESCVM and the other standard approaches for different step sizes and its specification is discussed in detail.

2. Governing equations (Navier-Stokes equations)

The momentum and continuity equations were applied to model the incompressible laminar flow regime as described in (Reddy 2014)

$$\rho \frac{\partial \mathrm{u}}{\partial t} + \rho u \cdot \nabla u = -\nabla P + f + \nabla \cdot \left[2\mu\gamma(u)\right] \tag{1}$$

$$\nabla \cdot u = 0 \tag{2}$$

Where u, ρ, P and, μ are the velocity, density, pressure and viscosity, respectively. t and f are the time and, the body force. $\gamma(u) = (\nabla u + \nabla u^T)/2$is the shear rate tensor. Eqs. (1) and (2) are completed with a suitable set of initial conditions

$$u(x, t=0) = U_0(x) \qquad \text{in } \Omega \tag{3}$$

And the Dirichlet and Neumann boundary conditions

$$u(x,t) = U_D(x,t) \quad on\ \Gamma_D \tag{4}$$

$$T = \left[-P\mathbf{I} + 2\mu\gamma(u)\right] \cdot \hat{n} = F^N \quad on \quad \Gamma_N \tag{5}$$

Where U_D and U_0 are the initial velocity and the velocity on the boundary $\Gamma_D$respectively. **I** and $F^N$are the identity matrix, and the specified boundary condition of the surface traction force (T) respectively.

3. Velocity- pressure analysis by FEA

Finite Element Analysis (FEA) assumes that every system consists of several components, called elements, and that the principles governing the system can be effectively applied to these individual parts. By integrating Eqs. (1) and (2) over an element for 2D domains and integrating by parts for velocity and pressure variables, Eqs. (6) to (10) are obtained (Reddy 2014)

$$\int_{\Omega^e} Q\left(\frac{\partial v_x}{\partial x}+\frac{\partial v_y}{\partial y}\right)dxdy = 0 \tag{6}$$

$$\int_{\Omega^e}\left(\begin{array}{l} w_x\rho\dfrac{\partial v_x}{\partial t}+w_x\rho\left(v_x\dfrac{\partial v_x}{\partial x}+v_y\dfrac{\partial v_x}{\partial y}\right)+2\mu\dfrac{\partial w_x}{\partial x}\dfrac{\partial v_x}{\partial x}+ \\ \mu\dfrac{\partial w_x}{\partial y}\left(\dfrac{\partial v_x}{\partial y}+\dfrac{\partial v_y}{\partial x}\right)+\dfrac{\partial w_x}{\partial x}P-w_x f_x \end{array}\right)dxdy - \oint_{\Gamma^e} w_x T_x ds = 0 \tag{7}$$

$$\int_{\Omega^e}\left(\begin{array}{l} w_y\rho\dfrac{\partial v_y}{\partial t}+w_y\rho_0\left(v_x\dfrac{\partial v_y}{\partial x}+v_y\dfrac{\partial v_y}{\partial y}\right)+2\mu\dfrac{\partial w_y}{\partial y}\dfrac{\partial v_y}{\partial y}+ \\ \mu\dfrac{\partial w_y}{\partial x}\left(\dfrac{\partial v_x}{\partial y}+\dfrac{\partial v_y}{\partial x}\right)+\dfrac{\partial w_y}{\partial y}P-w_y f_y \end{array}\right)dxdy - \oint_{\Gamma^e} w_y T_y ds = 0 \tag{8}$$

$$T_x = \left(2\mu\frac{\partial v_x}{\partial x}-P\right)n_x+\mu\left(\frac{\partial v_x}{\partial y}+\frac{\partial v_y}{\partial x}\right)n_y \tag{9}$$

$$T_y = \mu\left(\frac{\partial v_x}{\partial y}+\frac{\partial v_y}{\partial x}\right)n_x+\left(2\mu\frac{\partial v_y}{\partial y}-P\right)n_y \tag{10}$$

Where (n_x, n_y) are the directional cosines of the vector $\hat{n}$ at the boundary Γ^e. The components of the boundary traction stress are $T_x$and T_y. The dependent variables (P, v_x, v_y) can be estimated using Eq. (11).

$$v_x(x,y,t)=\sum_{m=1}^{M}\psi_m(x,y)v_x^m(t),\ v_y(x,y,t)=\sum_{m=1}^{M}\psi_m(x,y)v_y^m(t),\quad P(x,y,t)=\sum_{n=1}^{N}\phi_n(x,y)P_n(t) \tag{11}$$

The nodal values of (P, v_y, v_x) is (P_n, v_y^m, v_x^m), ψ and φ are shape functions. The weight functions (Q, w_y, w_x) is described in Eq. (12).

$$\begin{cases} w_x = v_x, \\ Q \approx P, \\ w_y \approx v_y, \end{cases} \tag{12}$$

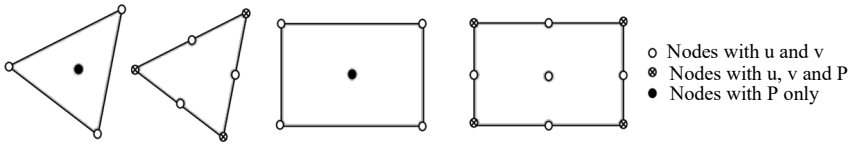

Fig. 1 The different elements for problem analysis by FEA

The above expression can be compressed into a bellows form

$$M\dot{U} + KU = F \tag{13}$$

Where $M, K$and F are obtained by substitution and arrangement of the terms. The elements used in this study are quadrilateral and triangular, that (v_x, v_y, P) is the set of nodal variables. The polynomial interpolation applied to the velocity and pressure variables must be different. It should be noted that in Eqs. (6) to (8) the weak forms only contain the FO derivatives of the velocity and not the pressure derivative. The pressure values are also not present in the essential boundary conditions, but they are satisfied as part of the natural conditions. Fig. 1 shows the elements that apply to the incompressible viscous fluids.

The Adams-Bashforth rule is used for transient solutions. The Adams-Bashforth predictor is given by Eq. (14).

$$U_p^{n+1} = U^n + \frac{\Delta t_n}{2}\left[\left(2 + \frac{\Delta t_n}{\Delta t_{n-1}}\right)\dot{U}^n - \left(\frac{\Delta t_n}{\Delta t_{n-1}}\right)\dot{U}^{n-1}\right] \tag{14}$$

Where $\Delta t_n = t_{n+1} - t_n$ and $\Delta t_{n-1} = t_n - t_{n-1}$

These formulas are used to predict the solution vector (without pressure), and they use two "acceleration" vectors from the previous time step. No matrix solution is required for this expression.

This is the compatible corrector formula for the above equation

$$\left[\frac{2}{\Delta t_n}M + K(U^{n+1})\right]U^{n+1} = \frac{2}{\Delta t_n}MU^n + M\dot{U}^n + F(U^{n+1}) \tag{15}$$

Eq. (15) can be solved iteratively to obtain the vector U^{n+1}. The following equation was used to calculate the vector $\dot{U}$ in the next time steps

$$\dot{U}^{n+1} = \frac{2}{\Delta t_n}(U^{n+1} - U^n) - \dot{U}^n \tag{16}$$

4. Sensitivity analysis

One of the essential questions in the design process is sensitivity analysis, which uses the application of a first- or second-order optimization method to determine the optimal variable and indicates which design variable is more significant at each step of the optimal variable. The discrete mathematical model corresponds to a physical problem explained in the form *R(x,w)=0* where w and $x \in \{x_1, x_2, \mathrm{L}\ , x_p\}^T$ represent the vector of state variables and a set of independent design variables, respectively. It is also assumed that the desired response is explained by the

function *f(x,w)*. The objective function f to be minimized or the constraints to be satisfied can be taken into account. Thus, the sensitivity analysis can be determined as the calculation of the Kth order partial derivative of *f* with respect to the independent variable x. Eq. (17) is the FO derivative of the objective function.

$$\nabla f = \left\{ \frac{\partial y}{\partial x_1}, \frac{\partial y}{\partial x_2}, \mathrm{L}\ , \frac{\partial y}{\partial x_p} \right\} \in R^p \tag{17}$$

Finite difference analysis, which is the simplest numerical technique for sensitivity calculations, is explained below. It can be considered as a traditional method for numerically calculating the derivatives of a function. The Finite difference method for sensitivity is determined by eliminating insignificant terms from the extended Taylor series of a function as follows (Chapra 2017).

$$f(x+\delta x) = f(x) + \delta x \frac{df}{dx} + \frac{\delta x^2}{2!}\frac{d^2 f}{dx^2} + \frac{\delta x^3}{3!}\frac{d^3 f}{dx^3} + \frac{\delta x^4}{4!}\frac{d^4 f}{dx^4} + \mathrm{L} \tag{18}$$

Eq. (19) is the forward finite difference estimation of the FO derivative.

$$\frac{df}{dx} \approx \frac{f(x+\delta x) - f(x)}{h} + O(\delta x) \tag{19}$$

The cut-off error associated with Eq. (19) is of order $O(\delta x)$. Therefore, this should be considered as a FO approximation. The auxiliary equations can be used with the extended Taylor series to reduce the cut-off error.

$$f(x-\delta x) = f(x) - \delta x \frac{df}{dx} + \frac{\delta x^2}{2!}\frac{d^2 f}{dx^2} - \frac{\delta x^3}{3!}\frac{d^3 f}{dx^3} + \frac{\delta x^4}{4!}\frac{d^4 f}{dx^4} - + \mathrm{L} \tag{20}$$

Subtracting Eq. (20) from Eq. (18) and solving for, yields the central difference approximation shown in Eq. (21)

$$\frac{df}{dx} \approx \frac{f(x+\delta x) - f(x-\delta x)}{2\delta x} + O\left(h^2\right) \tag{21}$$

Since the truncation error is equal to the SO, it can be shown that the accuracy of the SO can be achieved using the central difference method. However, this method requires the function to be evaluated twice, which is a prerequisite for the central difference approximation. The higher-order finite difference formula can also be constructed in this way. The higher order derivatives by finite difference approximation can be calculated by directly differentiating the lower order methods. As an illustration, the central difference approximation in Eq. (21) can be used to estimate the SO derivative.

$$\frac{d^2 f}{dx^2} \approx \frac{df(x+\delta x)/dx - df(x-\delta x)/dx}{2\delta x} + O(\delta x^2) \tag{22}$$

If we insert the corresponding formulas of $df(x+\delta x)/dx$ and $df(x-\delta x)/dx$, we get the following equation

$$\frac{d^2 f}{dx^2} \approx \frac{f(x+2\delta x)-2f(x)+f(x-2\delta x)}{4\delta x^2}+O(\delta x) \tag{23}$$

The expense in computations is order of the approximation dependent and increases linearly with the number of design variables. The accuracy of the approximation depends on the truncation error. In other words, with a small step size, any approximation error can be made small. In practice, however, the accuracy of the calculations is significantly influenced by the step size, which illustrates its crucial role in determining the overall reliability of the results.

The SCVM and the FDM are conceptually similar numerical differentiation methods. However, this method has considerable advantages over finite difference analysis. To explain the complex variables method, you should examine the analytical function f defined in terms of the complex variable x. The function f can be expressed by a Taylor series expansion centered on the real point x, as shown below

$$f(x+ih)=f(x)+ih\frac{df}{dx}-\frac{h^2}{2!}\frac{d^2 f}{dx^2}-\frac{ih^3}{3!}\frac{d^3 f}{dx^3}+\frac{h^4}{4!}\frac{d^4 f}{dx^4}-+\mathrm{L} \tag{24}$$

It must be pointed out that Eq. (24) was obtained by replacing h in Eq. (18) with ih, where $i^2=-1$. This method is known as the complex step approximation. The imaginary and the real parts (*Im* and R_e) of Eq. (24) can be considered as Eqs. (25) and (26).

$$Re\left[f(x+i\delta x)\right]=f(x)-\frac{\delta x^2}{2!}\frac{d^2 f}{dx^2}+O(h^4) \tag{25}$$

$$Im\left[f(x+i\,\delta x)\right]=\delta x\,\frac{df}{dx}-\frac{\delta x^3}{3!}\frac{d^3 f}{dx^3}+O(\delta x^5) \tag{26}$$

The FO derivative of the function *f*, which is given by Eq. (27), can be derived from Eq. (26) by dividing both sides by δx.

$$\frac{df}{dx}=\frac{Im\left[f(x+i\delta x)\right]}{\delta x}+O(\delta x^2) \tag{27}$$

The estimate derived from Eq. (27) provides an accurate representation of the FO derivative of the function f with respect to $O(\delta x^2)$. In contrast to the FDM, the upper estimate provides an approximation to the FO derivative that does not suffer from errors associated with the loss of significant figures since no subtraction is performed. It can be assumed that the main advantage of complex step estimation over FDM is that the issue of determining the appropriate step size has been successfully resolved. In principle, a minimum step size can be chosen without compromising the accuracy of the estimation.

It is important to note that Eq. (25) is used to obtain an approximation of the SO derivative. This is done as follows

$$\frac{d^2 f}{dx^2}=\frac{2\left(f(x)-Re\left[f(x+i\delta x)\right]\right)}{\delta x^2}+O(\delta x^2) \tag{28}$$

In contrast to the FO derivative estimation, Eq. (28) involves the subtraction operator, making its accuracy dependent on the chosen step size *h*.

Lai and Crassidis (2008) presented a refined formulation aimed at improving the precision of FO and SO sensitivities. Nevertheless, this formulation has not yet found application in the field of engineering. The complex unit vector holds potential for a number of applications. By applying standard principles of complex algebra, these vectors can be reformulated in the notation of $i^{(p/q)} = e^{i\beta}, (\beta = (p/q)\frac{\pi}{2})$.

In addition, the Taylor series, which contains two complex steps and a phase angle difference of π, can be expressed by Eqs. (29) and (30).

$$f\left(x+e^{i\beta}\delta x\right)=f\left(x\right)+\sum_{n=1}^{\infty}e^{ni\beta}\frac{\delta x^{n}}{n!}f^{(n)}\left(x\right) \tag{29}$$

$$f\left(x+e^{i(\beta+\pi)}\delta x\right)=f\left(x\right)+\sum_{n=1}^{\infty}e^{ni(\beta+\pi)}\frac{\delta x^{n}}{n!}f^{(n)}\left(x\right) \tag{30}$$

In the previous equations, an alternative method involves using the complex step *i* in its trigonometric form, as expressed by Euler's formula $e^{i\beta}=cos\,\beta+i\,sin\,\beta$, rather than its exponential form. This simplifies the derivation of the equations. By adding and subtracting Eqs. (29) and (30), we arrive at Eqs. (31) and (32)

$$f\left(x+e^{i\beta}\delta x\right)+f\left(x+e^{i(\beta+\pi)}\delta x\right)=\sum_{n=1}^{\infty}[cos\,2n\beta+i\,sin\,2n\beta]\frac{\delta x^{2n}}{(2n)!}f^{(2n)}\left(x\right)+2f\left(x\right) \tag{31}$$

$$f\left(x+e^{i\beta}\delta x\right)-f\left(x+e^{i(\beta+\pi)}\delta x\right)=2\sum_{n=1}^{\infty}\left[cos\,\beta(2n-1)+i\,sin\,\beta(2n-1)\right]\frac{\delta x^{2n-1}}{(2n-1)!}f^{(2n-1)}\left(x\right) \tag{32}$$

In order to achieve greater efficiency in this case, it is important to focus exclusively on the imaginary component.

$$Im\left(f\left(x+e^{i\beta}\delta x\right)+f\left(x+e^{i(\beta+\pi)}\delta x\right)\right)=2\sum_{n=1}^{\infty}sin\,2n\beta\frac{\delta x^{2n}}{(2n)!}f^{(2n)}\left(x\right) \tag{33}$$

$$Im\left(f\left(x+e^{i\beta}\delta x\right)-f\left(x+e^{i(\beta+\pi)}\delta x\right)\right)=2\sum_{n=1}^{\infty}sin\,\beta(2n-1)\frac{\delta x^{2n-1}}{(2n-1)!}f^{(2n-1)}\left(x\right) \tag{34}$$

By applying Eqs. (33) and (34), first and second order derivatives of each angle using the complex step method. Selecting the appropriate angles is crucial to fully utilize the extended complex variables method. A detailed analysis of Eqs. (33) and (34) shows cases where certain sine functions become zero, which can be used to improve the convergence rate of the Taylor series approximation. By choosing certain angles, it is possible to derive equations that are both practical and accurate. For example, the angles $\beta = 45°$and $\beta = 60°$are two different values that, when substituted into these equations, greatly simplify many of the coefficients in Eqs. (33) and (34).

In case 1, the substitution of $\beta = 45°$in Eq. (33) yields the following equation for the sensitivity of SO

$$f''(x)=\frac{Im\left(f\left(x+i^{1/2}\delta x\right)+f\left(x+i^{5/2}\delta x\right)\right)}{\delta x^{2}},E_{cut}\left(\delta x\right)=\frac{h^{4}}{360}f^{(6)}\left(x\right) \tag{35}$$

It is important to note that when $sin\,2\,n\beta = 0$ and n=2, the imaginary terms vanish. As a result, the first non-zero value occurs at n=3, which corresponds to $O(\delta x^4)$. Nevertheless, a subtraction error persists in the estimation. However, its cut-off error is $\delta x^4 f^{(6)}(x)/360$, and the associated error for Eq. (12) is $\delta x^2 f^{(4)}(x)/12$.

To compute the FO and SO derivatives utilizing Eqs. (27) and (35), it is essential to define $f(x+i\delta x), f\left(x+i^{1/2}\delta x\right)$ and $f\left(x+i^{5/2}\delta x\right)$.

To obtain the first-order derivative using $f\left(x+i^{1/2}\delta x\right)$ and $f\left(x+i^{5/2}\delta x\right)$, the value $\beta = 45°$ is substituted into Eq. (37), resulting in the following relation

$$f'(x) = \frac{Im\left(f\left(x+i^{1/2}\delta x\right) - f\left(x+i^{5/2}\delta x\right)\right)}{\sqrt{2}\delta x}, E_{cut}(\delta x) = -\frac{\delta x^2}{6} f^{(3)}(x) \tag{36}$$

It is important to emphasize that the error associated with Eq. (36) is identical to that of Eq. (27) and leads to comparable results. However, the same functions are used in Eq. (36) as in Eq. (34).

Due to $f\left(x+i^{1/2}\delta x\right) - f\left(x+i^{5/2}\delta x\right) = f\left(x+i^{1/2}\delta x\right) - f\left(x-i^{1/2}\delta x\right)$, the subtraction error is eliminated in Eq. (36), and the imaginary components are merged. A key aspect of Eqs. (35) and (36) is that the FO and SO derivatives are derived from two separate simulations, with the accuracy of the SO sensitivity being roughly fourth-order.

In Case 2, substituting $\beta = 60°$ in Eqs. (33) and (34) yields the FO and SO sensitivities, which are obtained by Eqs. (37) and (38).

$$f'(x) = \frac{Im\left(f\left(x+i^{2/3}\delta x\right) - f\left(x+i^{8/3}\delta x\right)\right)}{\sqrt{3}\delta x}, E_{cut}(\delta x) = \frac{\delta x^4}{120} f^{(5)}(x) \tag{37}$$

$$f''(x) = \frac{Im\left(f\left(x+i^{2/3}\delta x\right) + f\left(x+i^{8/3}\delta x\right)\right)}{\sqrt{3}\delta x}, E_{cut}(\delta x) = \frac{\delta x^2}{24} f^{(4)}(x) \tag{38}$$

It is clear that the equation for the first-order (FO) derivative is more accurate than that for the second-order (SO) derivative. Unlike the SO derivatives, which are prone to both subtraction and truncation errors, the FO derivatives do not suffer from subtraction errors. Therefore, the equations derived for this case ($\beta = 45°$), particularly Eqs. (35) and (36), are more suitable for calculating derivatives.

To implement the complex step method, it is crucial to first develop simulation code that does not already use complex arithmetic. In this scenario, to leverage the benefits of the complex variable method, an automated process can be used to generate enhanced code that can compute both the function and its derivatives.

In addition to the clear need for full access to the original code, developing an advanced version requires three phases, as shown in Fig. 2.

In this study, MATLAB software was used to carry out the three steps shown in Fig. 2. MATLAB can handle complex variables as standard input data, so the first step is relatively simple. However, it is important to point out that in the second step, determining the complex step size

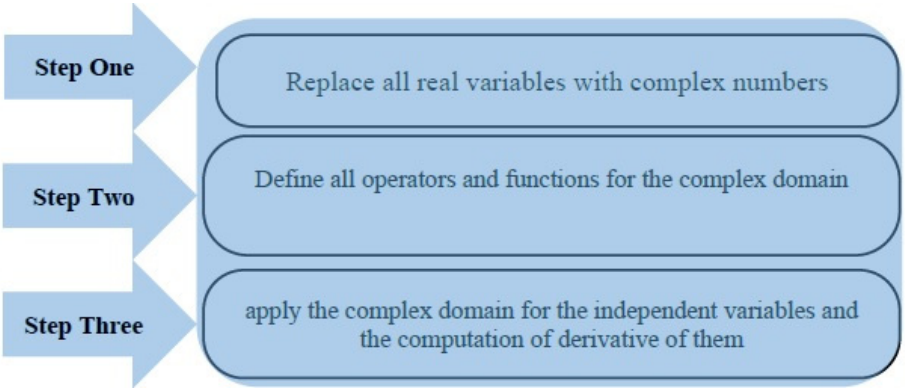

Fig. 2 The steps of producing a complex version of the code

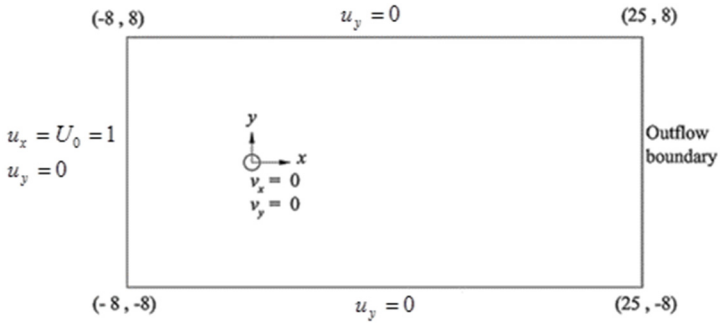

Fig. 3 Domain and boundary conditions for the flow around a circular cylinder

depends on the assumption that the function is analytic. Therefore, it is crucial to carefully check the correctness of this assumption when incorporating functions and operators in the complex domain. The last step can then be completed using the specified equations.

5. Numerical example

5.1 Flow around a cylinder

The method described above was used here to evaluate the flow around a cylinder at a high Reynolds number. The most significant challenge in this evaluation was the periodic flow regime. When the Reynolds number ($\mathrm{Re} = \rho U_0 d / \mu$) of the free flow exceeds $Re_c \approx 51$ (Sohankar *et al.* 1998), the flow becomes periodic.

A circular cylinder with a unit diameter within a specified range $\{\overline{\Omega} : -8 \le x \le 25, -8 \le y \le 8\}$ was assumed. The x-component of the velocity at the lower and upper walls, as well as at the inlet, was set to one, while the y-component of the velocity at these boundaries was considered zero (as

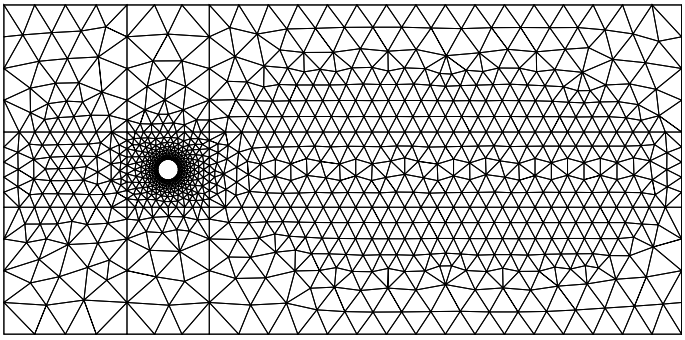

Fig. 4 Finite element mesh for the flow around a circular cylinder

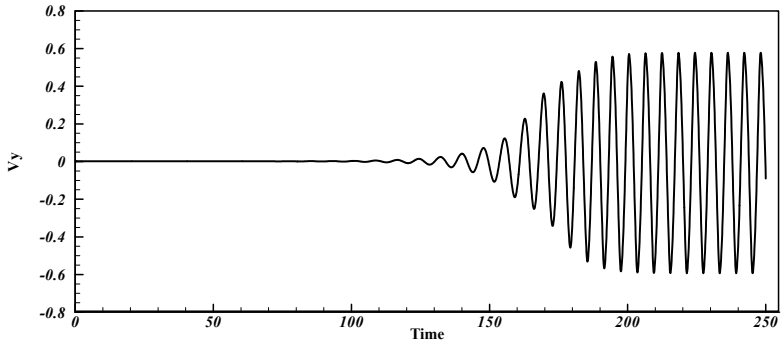

Fig. 5 Time history of v_y-velocity component for the flow around a circular cylinder at (*x*,*y*)=(2,0)

shown in Fig. 3). The Reynolds number was taken to be 100. The finite element mesh used in the calculations is depicted in Fig. 4, and it consists of triangular elements—six-node elements for the velocity and three-node elements for the pressure. The total number of elements was 1,815, with 3,733 nodes for velocity and 959 nodes for pressure. This mesh results in a total of 8,425 degrees of freedom. To study the temporal evolution of the velocity component as a function of time, the point *(x,y)=(2,0)* was chosen. A fixed time step of $\Delta t = 0.1$ was used, which was sufficient to verify and validate the solution. To speed up the convergence of the results, the solution obtained in the previous time step was used as an initial estimate for the current time step.

5.1.1 Verification

The temporal progression of the velocity component at the specified point *(x,y)=(2,0)*, along with the history of the drag coefficient, is shown in Figs. 5 and 6, respectively. From these figures, it can be observed that periodic flow begins at approximately $t = 120s$. Additionally, the time period measured from Fig. 6 is \dots, which yields a dimensionless flow frequency of $St = 0.1667$. Our results are in good agreement with the experimental findings of Hammache and Gharib (1991)($St = 0.166$). Fig. 7 presents the contour of the velocity component and vorticity at 130 seconds.

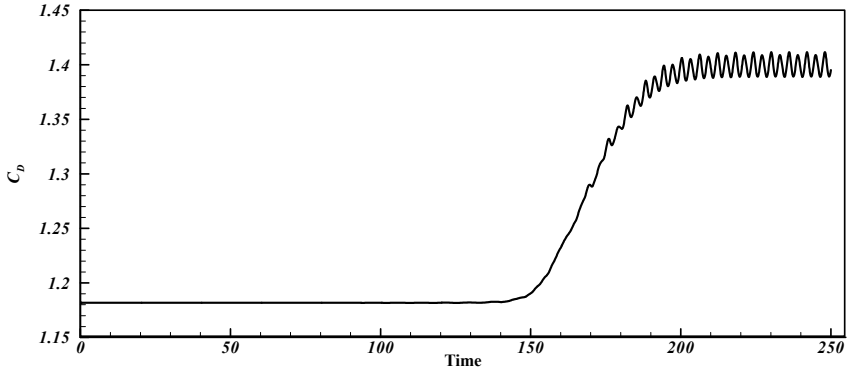

Fig. 6 Time history of C_D-drag coefficient for the flow around a circular cylinder

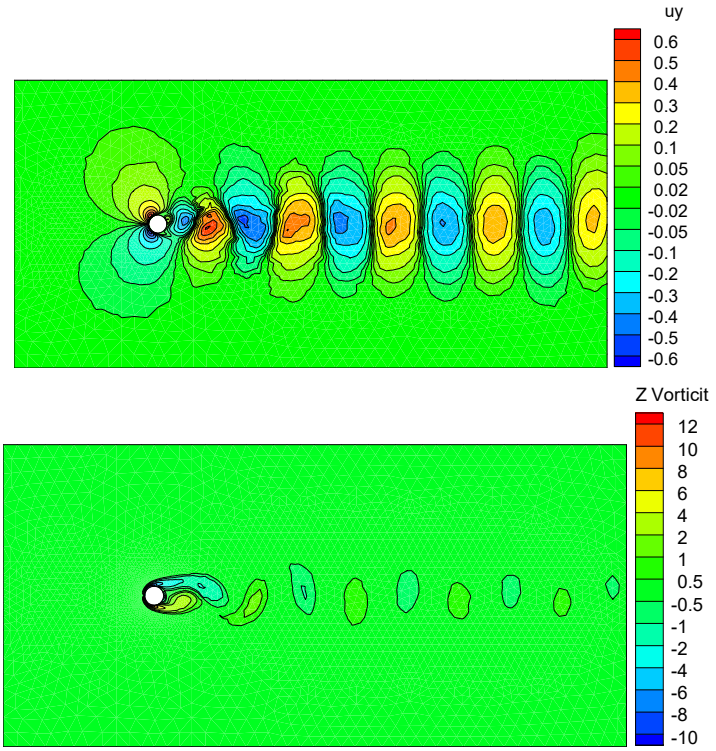

Fig. 7 Numerical results for flow around the cylinder (a) Vertical velocity contour (b) vorticity contour

5.1.2 Sensitivity analysis

In this section, sensitivities of the velocity fields and the pressure with respect to the input velocity U_0 were computed. Sensitivity computations depended on Eqs. (27) to (28) and (35) to (36), using the complex variables technique. With respect to this, the calculation of sensitivity implies a small variation in the value of the input velocity U_0, indicated as a step-size, rendered in the complex variable format.

Table 1 A comparative analysis of the sensitivity of the drag coefficient concerning the inlet velocity for both the FO and SO configurations ($\left(\frac{\partial C_D}{\partial U_0}, \frac{\partial^2 C_D}{\partial U_0^2}\right)$) for a flow passing around a cylinder at, t=200 s and R_e=100

step size	*FO*			*SO*		
	SCVM	*ESCVM*	*FDA*	*SCVM*	*ESCVM*	*FDA*
10^{-2}	*69.48641346372*	*69.48641425159*	*69.48641425163*	*0.11879785278*	*0.11879765762*	*0.11879746222*
10^{-4}	*69.48641385761*	*69.48641385769*	*69.48641385770*	*0.11879879303*	*0.11879765548*	*0.11879726092*
10^{-6}	*69.48641385765*	*69.48641385765*	*69.48641385152*	*0.12922996007*	*0.11879752959*	*0.10125233985*
10^{-8}	*69.48641385765*	*69.48641385765*	*69.48641378957*	*0.00000000000*	*0.11881542909*	*-2.91E+02*
10^{-10}	*69.48641385765*	*69.48641385765*	*69.48642439220*	*0.00000000000*	*0.11770780117*	*-4.66E+05*
10^{-12}	*69.48641385765*	*69.48641385765*	*69.48930320050*	*0.00000000000*	*0.22618219875*	*4.44E+08*
10^{-14}	*69.48641385765*	*69.48641385765*	*69.59988141375*	*0.00000000000*	*-2.01948391737*	*-5.11E+13*

$$U_0 = U_0 + i^n \delta x \tag{39}$$

When i^2 = -1, δx represents the disturbance (or step size) and is a small value assigned to the input velocity U0, virtually. This is not a real physical change in the input velocity, but rather a change in the complex number space that results in the calculation of the derivative of the function with very high accuracy and without the occurrence of subtraction error. In the standard complex variable method, n is equal to one, while in the extended form, n is set to 0.5 (in the case of $\theta = 45$). Table 1 demonstrates the first-order (FO) and second-order (SO) sensitivities for various step sizes using different forms, including finite difference analysis for validation.

To more clearly explain how the proposed method works, the following steps should be performed.

Step 1. run a Complex Simulation (Only One Simulation): The key is that we solve the Navier-Stokes equations (governing the flow) only once, but we do this solution in complex number space. In this simulation, we set the inlet velocity boundary condition not as a real number U_0, but as a complex number $U = U_0 + i\delta$.

Step 2. Calculating C_D in Complex Space: During this same solution, the finite element software (which now can work with complex numbers), when the input is in the form of complex numbers, all variables and results, including direct results (i.e., velocity and pressure fields) and computational results (such as CD, etc.) that depend on the velocity and pressure fields, are converted into complex numbers because it performs all the steps of calculating the flow field (velocity, pressure) and finally calculating quantities such as the drag coefficient (C_D) using complex numbers. Therefore, the output of this analysis will be a complex drag coefficient $C_D = C_D (U_0 + i\delta)$.

Step 3. Extracting the derivative of the imaginary part: According to the basic CVM relation (Eq. (27)), the first derivative of C_D with respect to U_0 is obtained by taking the imaginary part of the same complex output and dividing it by δ: $\frac{dC_D}{dU_0} \approx \frac{\mathrm{Im}[C_D(U_0 + i\delta)]}{\delta}$.

The sensitivity estimated using the complex variable method aligns well with results from the finite difference analysis. The complex variable method is particularly robust for first-order (FO) calculations, showing little sensitivity to small step sizes. This suggests that both methods can be applied effectively across a broader range of step sizes, producing stable and satisfactory results.

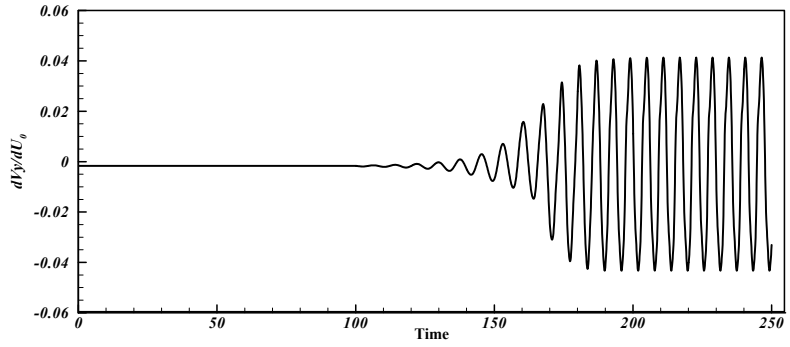

Fig. 8 The FO sensitivity of the vertical velocity concerning U_0, $\frac{\partial u_y}{\partial U_0}$ at (*x*,*y*)=(2,0) for flow around the cylinder with a high Reynolds number

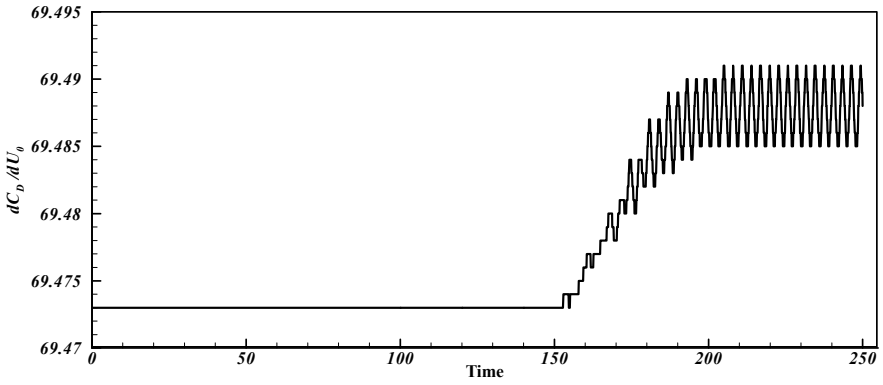

Fig. 9 The FO sensitivity of the drag coefficient concerning U_0, $\frac{\partial u_y}{\partial U_0}$ for flow around the cylinder with a high Reynolds number

All three approaches yield acceptable outcomes and show reduced sensitivity to cut-off errors when larger step sizes are used.

The second-order (SO) sensitivity to variations in input parameters, as estimated by the Extended Complex Variable Method (ECVM) and the Standard Complex Variable Method (SCVM), shows good agreement with the finite difference approach. It can be observed that SO sensitivity in all three methods is affected by both small and large step sizes. Notably, the ECVM demonstrates less sensitivity to step size variations than the other methods, resulting in a broader range of acceptable results. Additionally, the accuracy of SO sensitivity is more strongly influenced by step size, with the SCVM also showing some dependence on this choice. As a result, both rounding and cut-off errors were present.

Figs. 8 and 9 display the first-order (FO) sensitivities at point *(x,y)=(2,0)* and the drag coefficient over time. These sensitivities exhibit periodic behavior, mirroring the oscillatory nature of the flow components. The period of FO sensitivity is $\tau = 6s$, which exactly matches the period of the flow.

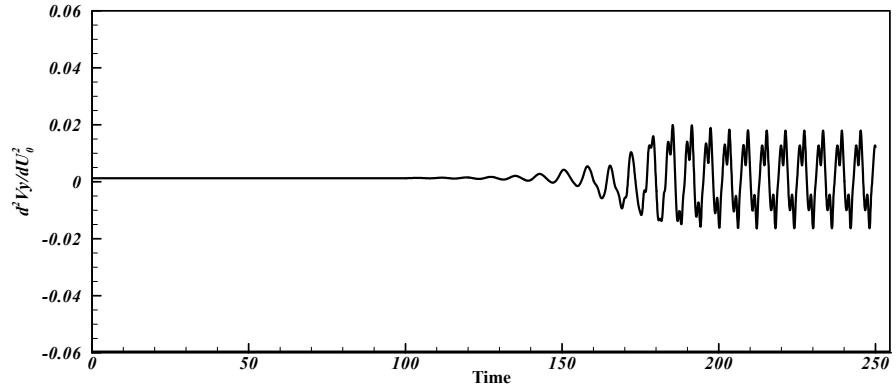

Fig. 10 The SO sensitivity of the vertical velocity concerning U_0, $\frac{\partial^2 u_y}{\partial U_0^2}$ at (*x*,*y*)=(2,0) for flow around the cylinder with a high Reynolds number

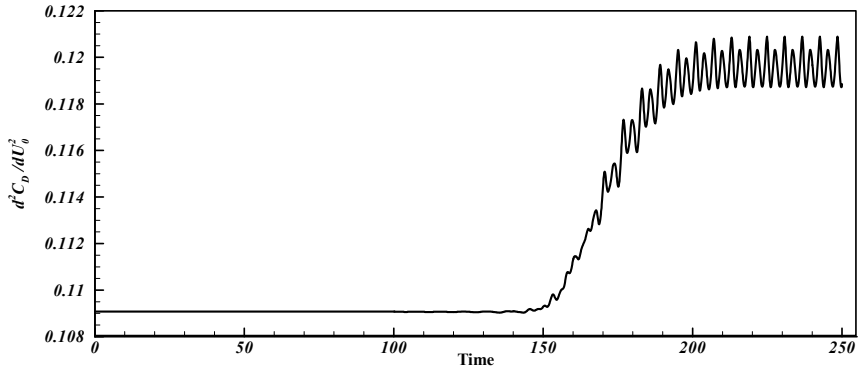

Fig. 11 The SO sensitivity of the drag coefficient concerning U_0, $\frac{\partial^2 C_D}{\partial U_0^2}$ for flow around the cylinder with a high Reynolds number

Figs. 10 and 11 plot the second-order (SO) sensitivities for u_y at point*(x,y)=(2,0)* and the drag coefficient over time. These sensitivities show periodic behavior similar to that of the flow components. The time period of the SO sensitivity matches that of the first-order (FO) sensitivity $\tau = 6s$ and is also equal to the time period of the flow.

5.2 Flow around the square cylinder with high Reynolds number

In this example, the flow around a square cylinder at a Reynolds number (*Re*) of 100 was evaluated. The Reynolds number is calculated based on the free-stream velocity (U_0) and the side length of the square (*L*).

The square cylinder has a unit length (*L*=1.0) and is positioned within the finite region $\{\overline{\Omega} : -10.5 \le x \le 25.5, -10.5 \le y \le 10.5\}$. The center of the square is located at *(x,y)=(0,0)*. For the

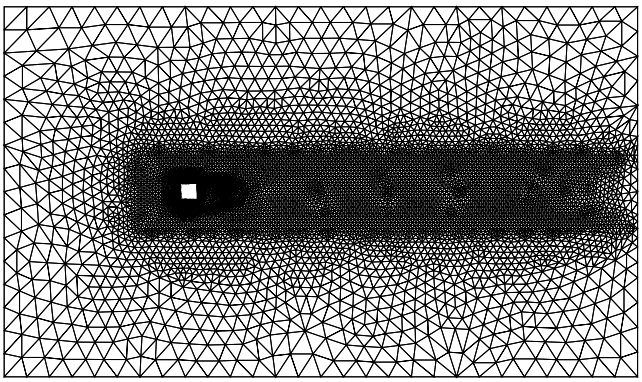

Fig. 12 finite element mesh for the flow around a square cylinder

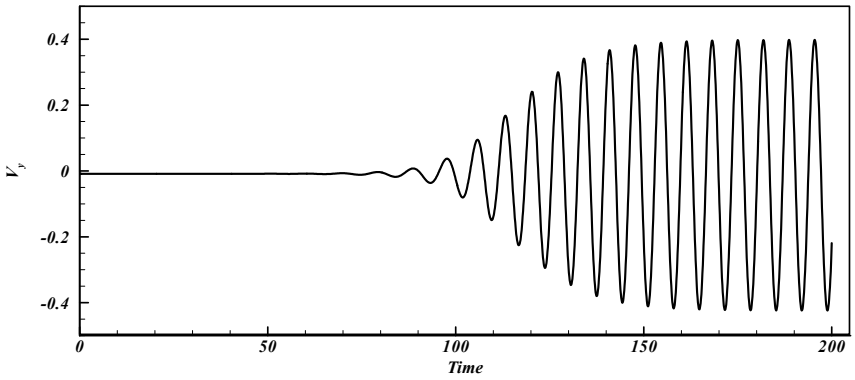

Fig. 13 Time history of v_y-velocity component for the flow around a square cylinder at (*x*,*y*)=(2,0)

boundary conditions, the *x*-component of velocity at the lower and upper walls, as well as the inlet flow, was set to one, while the y-component of velocity was set to zero at these boundaries.

The mesh used in the finite element analysis is shown in Fig. 12 and consists of six-node triangular elements for velocity and three-node triangular elements for pressure. The total number of elements is 6258, with 12,764 nodes for velocity and 3253 nodes for pressure. Point *(x,y)=(2,0)* was selected to observe the changes in the y-component of velocity v_y over time. A fixed time step of $\Delta t = 0.1s$ was assumed sufficient for verification and validation of the solution. To accelerate convergence, the solution from the previous time step was used as an initial estimate for solving the current time step.

5.2.1 Verification

Figs. 13 and 14 show the time history of the velocity component at point *(x,y)=(2,0)* and the time history of the drag coefficient, respectively. From these figures, it can be observed that the flow becomes periodic at approximately $t = 75s$. Furthermore, the time period measured from Fig. 13 is $\tau = 6.8s$, yielding a dimensionless flow frequency of $St = 0.147$. Table 2 presents the calculated parameters alongside experimental measurements by Okajima (1982) and numerical

Table 2 Comparison of computed for flow around the square cylinder at Re = 100

methods	*St*	$\overline{C}_D$	$\overline{C}_{Dp}$
Present study	0.147	1.505	1.407
Okajima (1982)	0.143±0.002	-	-
Sohankar *et al*. (1998)	0.146	1.46	1.414
Pavlov *et al. (2000)*	0.150	1.51	-
Pontaza and Reddy *(2006)*	0.140	1.48	1.382

Strouhal number St, average drag coefficient $\bar{C}_D$, average pressure drag coefficient $\bar{C}_{Dp}$

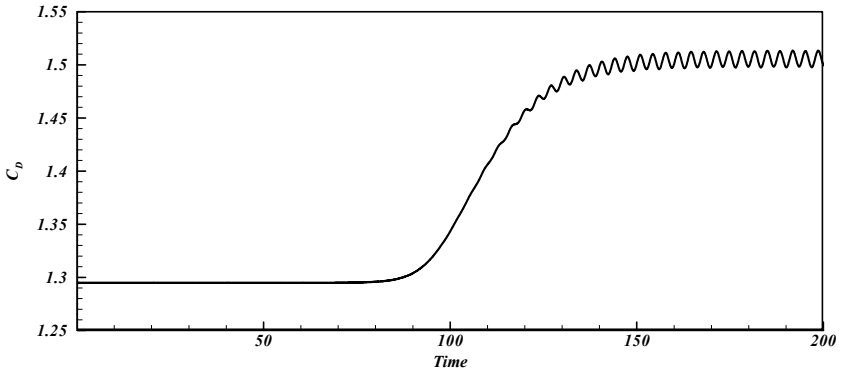

Fig. 14 Time history of C_D-drag coefficient for the flow around a square cylinder

results from Sohankar *et al.* (1998), Pavlov *et al.* (2000), and Pontaza and Reddy (2006) under the same flow conditions. The calculated dimensionless shedding frequency (St) aligns well with the measurements in reference Okajima (1982) and with results in references Sohankar *et al.* (1998) and Pavlov *et al.* (2000), though it is slightly lower. A strong agreement is also found for the computed values of drag coefficient $\bar{C}_D$and lift coefficient $\bar{C}_{Dp}$. Fig. 15 illustrates the contour of the velocity component $u_y$and vorticity at t=175 s.

5.2.2 Sensitivity analysis

Table 3 presents the first-order (FO) sensitivity for different step sizes using various methods, including finite difference analysis for validation. The sensitivity calculated by the standard complex variable method aligns well with the finite difference results. Notably, the standard complex variable method is unaffected by small step sizes, suggesting that both methods can be applied across a wide range of step sizes while still yielding reliable and satisfactory results. All three methods produce acceptable outcomes and show reduced dependence on cut-off errors when larger step sizes are used.

It can be observed that the second-order (SO) sensitivity to both small and large step sizes is similar across all three methods. However, the Extended Complex Variable Method (ECVM) is less sensitive than the other two, resulting in a broader range of acceptable results. An analysis of Tables 1 and 2 reveals that the accuracy of SO sensitivity is significantly affected by step size.

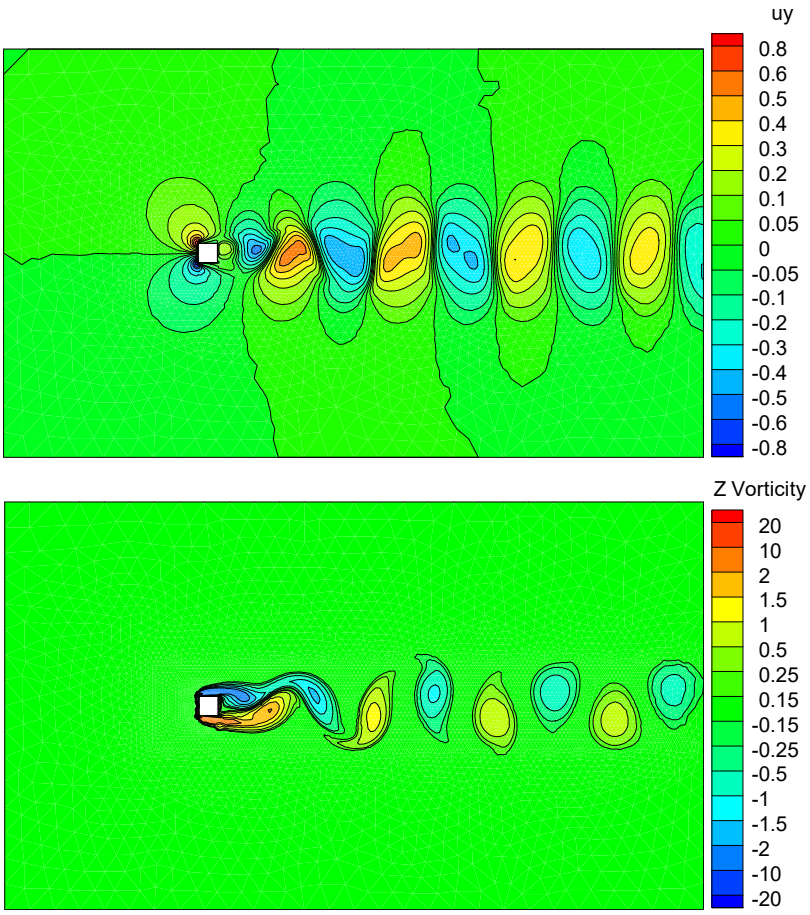

Fig. 15 Numerical results for flow around the cylinder (a) Vertical velocity contour (b) vorticity contour

Table 3 The analysis focuses on contrasting the sensitivity of the drag coefficient concerning the inlet velocity for both FO and SO configurations $\left(\frac{\partial C_D}{\partial U_0}, \frac{\partial^2 C_D}{\partial U_0^2}\right)$ for a flow passing around a square cylinder at, t=200 s and R_e=100

Step size	FO			SO		
	SCVM	ESCVM	FDA	SCVM	ESCVM	FDA
10^{-2}	95.68582747674	95.68588227169	95.68588227127	0.70285245082	0.70284537197	0.70283829428
10^{-4}	95.68585486567	95.68585487115	95.68585487114	0.70285435250	0.70285419481	0.70285421927
10^{-6}	95.68585486841	95.68585486841	95.68585487318	0.69366734579	0.70285423803	0.69655392565
10^{-8}	95.68585486841	95.68585486841	95.68585480624	-150.9903	0.70275994293	-59.9520
10^{-10}	95.68585486841	95.68585486841	95.68585812580	-2.04E+06	0.70120100526	6.66E+04
10^{-12}	95.68585486841	95.68585486841	95.69345316152	-1.29E+10	0.87887940084	4.00E+09
10^{-14}	95.68585486841	95.68585486841	95.95657601835	-1.69E+14	-24.2338	2.24E+14

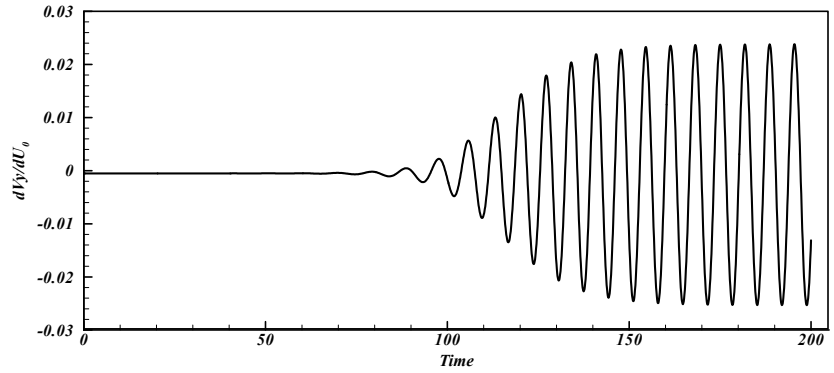

Fig. 16 The FO sensitivity of the vertical velocity relative to U_0, $\frac{\partial u_y}{\partial U_0}$ at (*x*,*y*)=(2,0) for flow around the square cylinder with a high Reynolds number

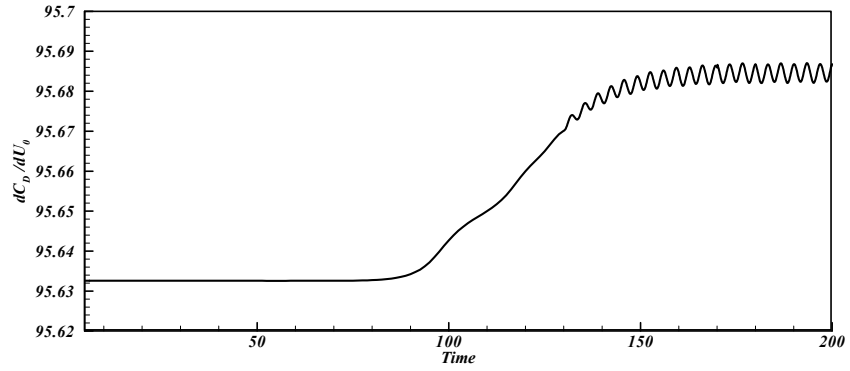

Fig. 17 The FO sensitivity of the drag coefficient concerning U_0, $\left(\frac{\partial C_D}{\partial U_0}\right)$ for flow around the square cylinder with a high Reynolds number

Additionally, the complex variable method for calculating SO sensitivity shows some dependence on step size. It is also important to note that both rounding and cut-off errors are evident in the results.

Figs. 16 and 17 illustrate the first-order (FO) sensitivities at point *(x,y)=(2,0)* and the drag coefficient C_D with respect to U_0 over time. The results in these figures reveal that these sensitivities exhibit periodic behavior, closely mirroring the periodicity of the flow components. Notably, the time period of the FO sensitivity, $\tau = 6.8s$ is identical to the time period of the flow, confirming synchronized temporal patterns.

Figs. 18 and 19 plot the second-order (SO) sensitivity of u_y at the specific point *(x,y)=(2,0)* and the drag coefficient concerning U_0 over time. These sensitivities show periodic behavior similar to the flow components. The time period of the SO sensitivity matches that of the first-order (FO) sensitivity $\tau = 6.8s$, which is also equal to the time period of the flow.

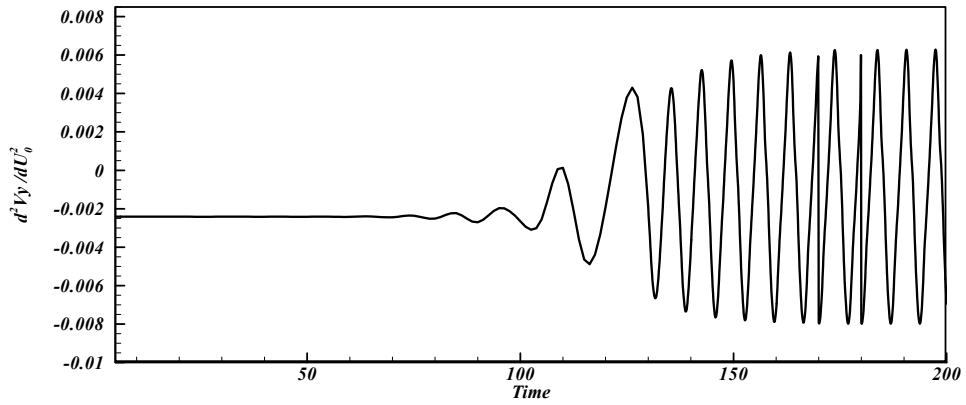

Fig. 18 The SO sensitivity of the vertical velocity concerning U_0, $\left(\frac{\partial^2 u_y}{\partial U_0^2}\right)$ at (x,y)=(2,0) for flow around the square cylinder with a high Reynolds number

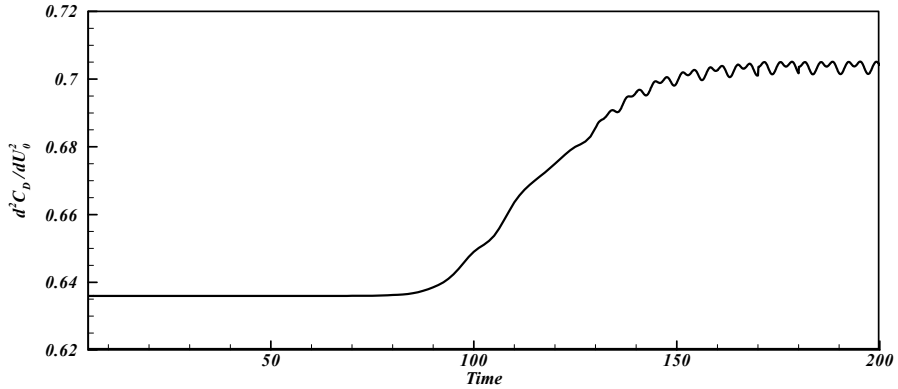

Fig. 19 The SO sensitivity of the drag coefficient concerning U_0, $\left(\frac{\partial^2 C_D}{\partial U_0^2}\right)$for flow around the square cylinder with a high Reynolds number

6. Conclusions

Given the importance of optimal design, identifying optimal parameters and utilizing sensitivity analysis in various engineering applications are essential. In this research project, the flow regime was initially modeled using finite element analysis (FEA). Subsequently, both first-order (FO) and second-order (SO) sensitivity analyses were conducted and evaluated within a transient flow regime. Complex variable methods were applied to estimate the FO sensitivity, while the Extended Complex Variable Method (ECVM) was used to determine the SO sensitivity.

These sensitivity analyses were then applied to flows around both a cylinder and a square. The results demonstrated that the flow regime was effectively captured through finite element analysis, and the sensitivity analysis results were consistent with traditional methods, yielding a

comprehensive set of valid results. The primary findings can be summarized as follows:

First, the extended and standard complex variable methods demonstrate independence from small step sizes regarding first-order (FO) sensitivity, achieving highly accurate results.

Second, in the flow around both a cylinder and a square, the flow regime becomes periodic above the critical Reynolds number. Similarly, both first-order (FO) and second-order (SO) sensitivities exhibit periodic behavior in alignment with the flow regime.

Third, while FO sensitivity remains relatively stable, SO sensitivity is more significantly impacted by step size.

Fourth, compared to other methods, the extended complex variable approach achieves more accurate SO sensitivity results, attributed to its capacity for larger step sizes.

Fifth, the standard complex variable method is recommended when the objective is solely to assess FO sensitivity, as it delivers high precision without concerns over step size. Conversely, the extended complex variable method (ESCVM) is preferable for calculating SO sensitivity, as it allows accurate determination of both FO and SO sensitivities with only two modeling runs.

Sixth, the extended complex variable method proves to be an effective approach for sensitivity analysis, showcasing its suitability in addressing engineering challenges.

References

Akkari, N., Hamdouni, A., Liberge, E. and Jazar, M. (2014), "A mathematical and numerical study of the sensitivity of a reduced order model by POD (ROM–POD), for a 2D incompressible fluid flow", *J. Comput. Appl. Math.,* **270**, 522-530. https://doi.org/10.1016/j.cam.2013.11.025.

Burg, C. and Newman, J. (2003), "Computationally efficient, numerically exact design space derivatives via the complex Taylor's series expansion method", *Comput. Fluids*, **32**(3), 373-383. https://doi.org/10.1016/S0045-7930(01)00044-5.

Chapra, S.C. (2017), *Applied Numerical Methods with MATLAB for Engineers and Scientists*, 4th Ed., McGraw-Hill.

Ding, Z., Li, L., Li, X. and Kong, J. (2018), "A comparative study of design sensitivity analysis based on adjoint variable method for transient response of non-viscously damped systems", *Mech. Syst. Signal Pr.,* **110**, 390-411. https://doi.org/10.1016/j.ymssp.2018.03.043.

Fiorini, C., Després, B. and Puscas, M.A. (2021), "Sensitivity equation method for the Navier-Stokes equations applied to uncertainty propagation", *Int. J. Numer. Meth. Fl.*, **93**(1), 71-92. https://doi.org/10.1002/fld.4875.

Hammache, M. and Gharib, M. (1991), "An experimental study of the parallel and oblique vortex shedding from circular cylinders", *J. Fluid. Mech*., **232**, 567-590. https://doi.org/10.1017/S0022112091003804.

Hu, G. and Kozlowski, T. (2018), "Application of continuous adjoint method to steady-state two-phase flow simulations", *Ann. Nucl. Energy*, **117**, 202-212. https://doi.org/10.1016/j.anucene.2018.03.029.

Ilinca1, F., Pelletier, D. and Hay, A. (2008), "First- and second-order sensitivity equation methods for value and shape parameters", *Int. J. Numer. Meth. Fl.*, **57**, 1349-1370. https://doi.org/10.1002/fld.1744.

Jafari, M. and Jafari, M. (2019), "Thermal stress analysis of orthotropic plate containing a rectangular hole using complex variable method", *Eur. J. Mech. Solid*, **73**, 212-223. https://doi.org/10.1016/j.euromechsol.2018.08.001.

Kavvadias, I.S., Papoutsis-Kiachagias, E.M. and Giannakoglou, K.C. (2015), "On the proper treatment of grid sensitivities in continuous adjoint methods for shape optimization", *J. Comput. Phys.*, **301**, 1-18. https://doi.org/10.1016/j.jcp.2015.08.012.

Lai, K.L. and Crassidis, J. (2008), "Extensions of the first and second complex-step derivative approximations", *J. Comput. Appl. Math*, **219**(1), 276-293. https://doi.org/10.1016/j.cam.2007.07.026.

Lambert, J. and Gosselin, L. (2018), "Sensitivity analysis of heat exchanger design to uncertainties of correlations", *Appl. Therm. Eng.,* **136**, 531-540. https://doi.org/10.1016/j.applthermaleng.2018.03.037.

Liu, G., Geier, M., Liu, Z., Krafczyk, M. and Chen, T. (2014), "Discrete adjoint sensitivity analysis for fluid flow topology optimization based on the generalized lattice Boltzmann method", *Comput. Math. Appl*., **68**(10), 1374-1392.

Martins, J.R., Kroo, I. and Alonso, J. (2000), "An automated method for sensitivity analysis using complex variables", *Proceedings of the 38th Aerospace Sciences Meeting and Exhibit*.

Martins, J.R., Sturdza, P. and Alonso, J.J. (2003), "The complex-step derivative approximation", *ACM Trans Math Soft*, **29**(3), 245-262.

Martins, J.R. and Hwang, J.T. (2013), "Review and unification of methods for computing derivatives of multidisciplinary computational models", *AIAA J*., **51**(11), 2582-2599. https://doi.org/10.2514/1.J052184.

Okajima, A. (1982), "Strouhal numbers of rectangular cylinders", *J. Fluid Mech*., **123**, 379-398. https://doi.org/10.1017/S0022112082003115.

Pavlov, A.N., Sazhin, S.S., Fedorenko, R.P. and Heikal, M.R. (2000), "A conservative finite difference method and its application for the analysis of a transient flow around a square prism", *Int. J. Numer. Method. H.*, **10**(1), 6-47. https://doi.org/10.1108/09615530010306894.

Pontaza, J.P. and Reddy, J.N. (2006), "Least-squares finite element formulations for viscous incompressible and compressible fluid flows", *Comput. Method. Appl. M.*, **195**, 2454-2494. https://doi.org/10.1016/j.cma.2005.05.018.

Reddy, J.N. (2014), *An Introduction to Nonlinear Finite Element Analysis: with applications to heat transfer, fluid mechanics, and solid mechanics*, 2th Ed., Oxford University Press.

Rodriguez, D. (2000), "A multidisciplinary optimization method for designing inlets using complex variables", *Proceedings of the 8th Symposium on Multidisciplinary Analysis and Optimization.*

Sheikhi Azqandi, M. (2021), "A novel hybrid genetic modified colliding bodies optimization for designing of composite laminates", *Mech. Adv. Compos. Struct.*, **8**, 203-212. https://doi.org/10.22075/macs.2020.20281.1254.

Sheikhi Azqandi, M., Nooredin, N. and Ghoddosian, A. (2018), "Optimization of spring back in U-die bending process of sheet metal using ANN and ICA", *Struct. Eng. Mech.*, **65**(4), 447-452. https://doi.org/10.12989/sem.2018.65.4.447.

Sheikhi Azqandi, M. and Hassanzadeh, M. (2018), "Computation of shape design sensitivities on thermo-elastic problems using modified semi-analytical method", *J. Mech. Eng. Univ Tabriz*, **48**(3), 155-164.

Sheikhi Azqandi, M., Hassanzadeh, M. and Arjmand, M. (2019), "Sensitivity analysis based on complex variables in FEM for linear structures", *Adv. Comput. Des*., **4**(1), 15-32. https://doi.org/10.12989/acd.2019.4.1.015.

Sheikhi Azqandi, M., Hassanzadeh, M. and Arjmand, M. (2020), "Calculation of design shape sensitivity in solid mechanics through a novel hybrid method using CVM and DSM", *J. Stress Anal.*, **5**(1), 11-20. https://doi.org/10.22084/jrstan.2020.21422.1142.

Sheikhi Azqandi, M. and Hassanzadeh, M. (2021), "First- and second-order sensitivity analysis of finite element models using extended complex variables method", *Arch. Appl. Mech.*, **91,** 4263-4277. https://doi.org/10.1007/s00419-021-01996-0.

Sohankar, A., Norberg, C. and Davidson, L. (1998), "Low-Reynolds-number flow around a square cylinder at incidence: study of blockage, onset of vortex shedding and outlet boundary condition", *Int. J. Numer. Meth. Fl.*, **26**(1), 39-56. https://doi.org/10.1002/(SICI)1097-0363(19980115)26:1<39::AID-FLD623>3.0.CO;2-P.

Squire, W. and Trapp, G. (1998), "Using complex variables to estimate derivatives of real functions", *SIAM Rev*., **40(**1), 110-112.

Ta, T.T.M., Le, V.C. and Pham, H.T. (2018), "Shape optimization for Stokes flows using sensitivity analysis and finite element method", *Appl. Numer. Math*., **126**, 160-179. https://doi.org/10.1016/j.apnum.2017.12.009.

Tanaka, M., Sasagawa, T., Omote, R., Fujikawa, M., Balzani, D. and Schröder, J. (2015), "A highly accurate

1st- and 2nd-order differentiation scheme for hyperelastic material models based on hyper-dual numbers", *Comput Method. Appl. M*., **283**, 22-45. https://doi.org/10.1016/j.cma.2014.08.020.

Tanaka, M., Balzani, D. and Schröder, J. (2016), "Implementation of incremental variational formulations based on the numerical calculation of derivatives using hyper dual numbers", *Comput. Method. Appl. M.*, **301**, 216-241. https://doi.org/10.1016/j.cma.2015.12.010.

Vincent, H. and Bogey, C. (2023), "Application of the complex differentiation method to the sensitivity analysis of aerodynamic noise", *Comput. Fluids*, **264**, 105965. https://doi.org/10.1016/j.compfluid.2023.105965Get rights and content.

Voorhees, A., Millwater, H., Bagley, R. and Golden, P. (2012), "Fatigue sensitivity analysis using complex variable methods", *Int. J. Fatigue,* **40**, 61-73. https://doi.org/10.1016/j.ijfatigue.2012.01.016.

MK